WELDING RESEARCH

SUPPLEMENT TO THE *WELDING JOURNAL,* JUNE 2015
Sponsored by the American Welding Society and the Welding Research Council

Ultrasonic Soldering Aluminum at Low Temperature

Strength and elongation of soldered joints can be improved with tin-based solder containing zinc

BY W. B. GUO, X. S. LENG, J. C. YAN, AND Y. M. TAN

ABSTRACT

A majority of aluminum alloys are heat sensitive and preferably joined at low temperature to avoid deterioration of mechanical properties. Tin- (Sn-) based solders with low melting points are very attractive for the joining of heat-sensitive aluminum alloys. In this study, ultrasonic soldering of pure Al at 300°C was investigated with Sn-based solders. The tensile strength of the joints only reaches 63± 2.8 MPa if using pure Sn as solder, and the joints fail along the interface between Al/Sn during the tensile test. However, if using Sn-Zn alloys, the tensile strength could be raised up to more than 80 MPa, and the joints fail in the filler metal layer. For Sn-9Zn and Sn-20Zn solders, joints all fail at the interface of Zn-rich and Sn-Zn eutectic phases in the bond metal. For hypoeutectic solder, the joints fail across b-Sn and Sn-Zn eutectic phase, and have maximum elongation. It indicates that Zn can strengthen the interface between the base metal and the solder through forming an Al-based solid solution layer containing Zn and Sn. The thickness of the solid solution increases with the content of Zn in the solder, but the strength of joints does not increase. Interface stronger than filler metal and best ductility could be realized with 4 wt-% Zn.

KEYWORDS

• Ultrasonic Soldering • Pure Al • Sn-based Solder • Microstructure
• Mechanical Properties

Introduction

Aluminum and its alloys have been widely used in aerospace, aircraft, and automobile applications for their high specific strength, excellent thermal conductivity, and heat treatability (Refs. 1–3). A key process for joining aluminum alloys is brazing, especially for relatively low bonding temperature and low residual stress applications (Ref. 4). The Al-Si and Zn-Al alloys are the most popular filler metals for aluminum (Refs. 5–7), and their melting points are still high for the deformation-strengthening and heat-treated aluminum alloys such as 2024 Al and 7075 Al (Refs. 8, 9), whose softening temperatures are 502°C and 465°C, respectively. Aluminum alloys and their composites are also used in electronic components and packaging (Ref. 10). In other applications, aluminum alloys need to be joined with temperature-sensitive materials (Ref. 11), which restricts brazing temperature. Some components like the superfluid helium dewar refrigerating machine for aircraft and spacecraft have special requirements for soldering temperatures as low as 200°–300°C, thus, low-temperature soldering for aluminum should be developed (Ref. 12). Sn-based solders have great potential for joining aluminum alloys (Ref. 13) because of their relatively lower melting points, but it is difficult to realize reliable metallic bonding between Sn and Al. First, without proper flux with a corresponding melting point, the oxide film of aluminum cannot be removed effectively. Second, the Al/Sn interface strength is quite low.

An ultrasonic wave in liquid solder can generate ultrasonic cavitation, and a microjet resulting from cavitation bubble implosion contributes to the breakage of oxide film. Chen (Ref. 14) estimated that the shock pressure of the microjet in Al-Si liquid alloys could reach about 0.78 GPa. Aluminum, titanium, and steel (Refs. 15–18) were all successfully joined by ultrasonic soldering. Faridi (Ref. 19) ultrasonic soldered 2024 Al with tin, and the joints achieved shear strength of only 38 MPa. Diao (Ref. 20) deposited a Cu-Ni adhesion film on the surface of aluminum, then joined the aluminum alloy by hot-dipping tin, thus achieving a Cu/Sn interface instead of a weak direct Al/Sn interface; however, the shear strength was as low as 40 MPa. Li (Ref. 13) found that aluminum dendrites migrating into the solder can strengthen the joint, and the maximum shear strength of a joint could approach 60 MPa. Ding (Ref. 21) sol-

W. B. GUO, X. S. LENG, J. C. YAN (jcyan@hit.edu.cn), and Y. M. TAN are with the State Key Laboratory of Advanced Welding and Joining, Harbin Institute of Technology, Harbin, China.

dered 6061 Al with ultrasonic Sn-Pb-Zn coating, and the highest shear strength was only 25 MPa. All of these works confirm weak metallic bonding between Al and Sn.

Recently, Sn-Zn solders have been used to join aluminum alloys to get higher strength. Nagaoka (Ref. 12) ultrasonic soldered 1070 Al under the liquidus temperature of Sn-Zn hypereutectic solder. However, few works focused on soldering aluminum with hypoeutectic Sn-Zn solder, which makes it difficult to understand the strengthening mechanism of Zn to Al/Sn interface and the relationship between content of Zn and mechanical properties of the joints. So in this work, pure Sn, hypoeutectic Sn-4Zn, eutectic Sn-9Zn, and hypereutectic Sn-20Zn filler metals were used to solder aluminum alloys at 300°C. Pure Al 1060 was chosen as the base metal for it can provide results to compare other Al alloys. Ultrasonic waves were used to break the oxide film and promote wetting and bonding between solder and base metal. The relationship between the Zn content, the microstructure, and mechanical properties were investigated. It helps in the selection of solder alloys and processing to realize high-strength metallic bonding of aluminum alloys at relatively low temperatures.

Experimental Procedures

Materials

The aluminum substrate used in this work is 9-mm-thick 1060 pure Al (supplied by Dongbei Light Alloys Co. Ltd.), whose chemical composition (wt-%) is shown in Table 1. The tensile strength of 1060 pure Al is 85± 0.8 MPa, and has no obvious change after the soldering thermal cycle.

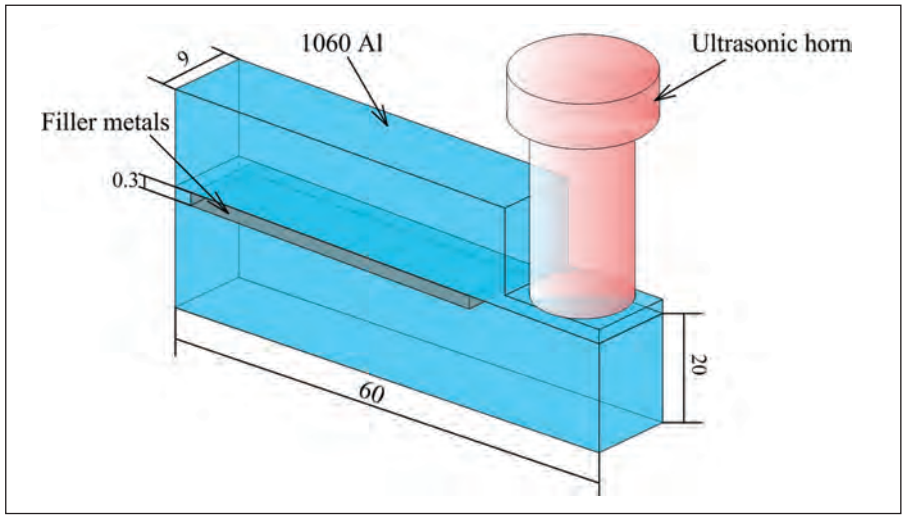

Fig. 1 — Schematic of ultrasonic soldering process.

Commercially pure tin (99.9%) was used as a filler metal. Pure tin and pure Zn (99.9%) were used to prepare Sn-Zn solders in a Al_2O_3 crucible at about 500°C. The chemical composition, and solidus (T_S) and liquidus (T_L) temperatures of the filler metals and three eutectic phases are shown in Table 2.

Soldering Process

The schematic diagram of the soldering process is shown in Fig. 1. The dimensions of the lower sample is 60 × 20 × 9 mm, and filler metal thickness of 300 μm was ensured by milling. The 1060 Al substrate was mechanically polished using 500-grit SiC papers. Then the polished substrate was ultrasonically cleaned in acetone for 10 min. A self-assembled ultrasonic soldering system equipped with ultrasonic equipment and heating units was used in this work. The frequency of the ultrasonic vibration was 20 kHz, with power of 1 kW and amplitude of 6.5 μm. All samples were heated to 300°C in air, and the temperature was measured with K-type thermocouples. Ultrasonic vibration was applied for 40 s, and the holding time was 10 min. Vibration direction of the horn was perpendicular to the soldering surfaces. The samples were removed from the heating platform and cooled in air.

Table 1 — Chemical Composition of 1060 Al

Material	Chemical Composition in wt-%							
	Cu	Mg	Mn	Fe	Si	Zn	Ti	Al
1060 Al	0.10	0.01	0.01	0.50	0.07	0.01	0.02	Bal.

Table 2 — Chemical Composition; Solidus and Liquidus emperatures of Filler Metals and Some Phases

Filler Metals or Phases	Chemical Composition in wt-%			Solidus and Liquidus Temperature in °C	
	Sn	Zn	Al	T_S	T_L
Pure Sn	100	0	0	232	232
Sn-4Zn	95.89	4.11	0	198.5	212
Sn-9Zn	90.55	9.45	0	198.5	202
Sn-20Zn	79.64	20.36	0	198.5	277
Sn-Zn eutectic	91.2	8.8	0	198.5	198.5
Al-Sn eutectic	99.4	0	0.6	232	232
Al-Zn eutectic	0	6	94.0	381	381

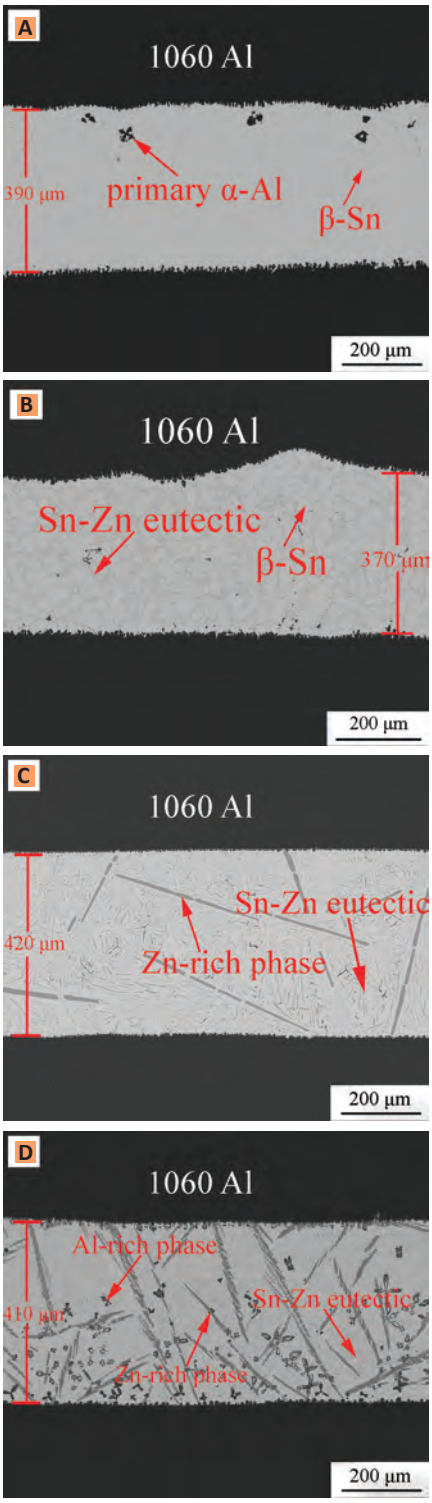

Fig. 2 — Microstructure of joints of 1060 Al soldered with A — pure Sn; B — Sn-4Zn; C — Sn-9Zn; D — Sn-20Zn.

Microstructure and Mechanical Testing

The sample for microstructure observation was prepared using standard polishing techniques. The joint microstructure, fracture location, and morphology of the fracture surface were observed by scanning electron microscopy (SEM:S3400, FEI-Quanta 200F) equipped with an energy-dispersive X-ray spectrometer (EDS). The joint tensile strength was evaluated with a tension testing machine (Instron-5569) at a constant speed of 0.5 mm/min. Three samples were used to calculate the average tensile strength. Elongation of the joint was used to evaluate the ductility, and elongation d is defined as follows:

$$d = (l_1 - l_0)/l_0 = \Delta l/l_0 \times 100\% \quad (1)$$

where l_0 is the original length of the joint, and l_1 is the joint's length after fracture.

Results and Discussion

Microstructure of Joints

Aluminum reacts with oxygen to form a layer of alumina at any temperature, which has to be removed before a metallic bond can be formed with Sn-based solder. Ultrasonic vibration can remove the oxide film effectively. Figure 2A shows the morphology of Al 1060/Sn joint. The interface is curved with some dissolution pits, which indicates that the aluminum oxide film was removed completely. A sound joint is realized without any obvious defects. The filler metal layer is mainly composed of b-Sn, Sn-Al eutectic, and primary a-Al phase. The chemical composition of the whole bond zone is Al: 2.67 % and Sn: 97.33%, based on EDS analysis. The solder and base metal dissolve each other after the oxide film is removed, but Sn and Al have very limited mutual solubility. At 300°C, the solubility of Al in pure Sn is about 1% according to the Al-Sn phase diagram (Ref. 22). The ultrasonic process can promote nucleation of the high-temperature phase (Ref. 23). After the liquid Sn is saturated with dissolved Al, a-Al, which is the high-temperature phase, will crystallize from liquid Sn, which makes liquid Sn subsaturated. At the same time, the ultrasonic process can accelerate dissolution by the stirring effect of acoustic streaming (Ref. 24), and Al will transfer into liquid Sn continuously to make liquid Sn saturated all the time. Therefore, Al content in the metallic bond zone exceeds the saturated solid solubility of Al in Sn at 300°C. The composition of Sn-Al eutectic is 0.6% Al and the eutectic temperature is 228°C. b-Sn and Sn-Al phase eutectic forms in the process of cooling.

Figure 2B shows the microstructure of the joint with the Sn-4Zn hypoeutectic solder. The microstructure of the bond zone mainly consists of b-Sn, Sn-Zn eutectic, and primary a-Al phase. The eutectic temperature of Sn-Zn is 198°C, so the a-Al and b-Sn phases are all pre-eutectic phase. b-Sn phase crystallizes first, and Sn-Zn eutectic phase fills in the gaps between the b-Sn particles. The chemical composition of Sn-Zn eutectic phase is Zn: 10.14%, and Sn: 89.96% by EDS analysis. The morphology of the joint with Sn-9Zn eutectic solder is shown in Fig. 2C. There are mainly Sn-Zn eutectic, Zn-rich, and a-Al phases. Zn hardly dissolves Sn at any temperature according to the Sn-Zn phase diagram (Ref. 25). Therefore, a-Al and Zn-rich phases can form during holding time. The chemical composition of Zn-rich phase is Zn: 98.40% and Sn: 1.60%. The joint with Sn-20Zn (Fig. 2D) has basically the same phase constitution as the joint with Sn-9Zn, but with more a-Al and Zn-rich phases. Also, more Al dissolves into the filler metal layer for larger mutual solubility of Zn and Al, and most of a-Al particles have a morphology of a petal shape.

Figure 3A–D shows the interface morphology of joints with pure Sn, Sn-4Zn, Sn-9Zn, and Sn-20Zn, respectively. When 1060 Al is soldered with pure Sn, a large amount of primary a-Al particles grow at the interface, with morphology of regular shape, as shown in Fig. 3A. During the time of holding and cooling, primary a-Al will crystallize from liquid tin, and prefers to nucleate at the aluminum base metal for lower nucleation energy. The corresponding EDS line-scanning result shows that the content of the elements changes dramatically at the interface, which indicates there is only a very thin diffusion layer of Al and Sn for their limited mutual solubility. With regard to the Sn-Zn soldered samples, the element distribution of the interface shows there are thicker

diffusion layers of elements than Al/Sn interface.

Figure 3B shows that Zn segregates at the interface with Sn-4Sn, indicating that Al-rich phase solid dissolves certain content of Zn, forming a solid solution of AlZnSn. When soldered with Sn-9Zn, Zn content and thickness of the solid solution increase — Fig. 3C. What's more, Zn has already diffused into the base metal through grain boundaries with Sn-20Zn solder — Fig. 3D. Al could dissolve about 0.5% of Zn, and Sn could hardly dissolve Zn at room temperature, according to Zn-Al (Ref. 26) and Sn-Zn phase diagrams. Therefore, Zn prefers to exist in an Al-rich phase at the interface.

Moreover, when primary a-Al crystallizes from liquid tin, it shows obvious anisotropy, and would like to present certain crystal faces outside to reduce its total surface free energy, and the Al-rich phase will lose its anisotropy for mutual dissolution of Al and Zn, resulting in a morphology of quasi-sphere at the interface with Sn-20Zn filler metal.

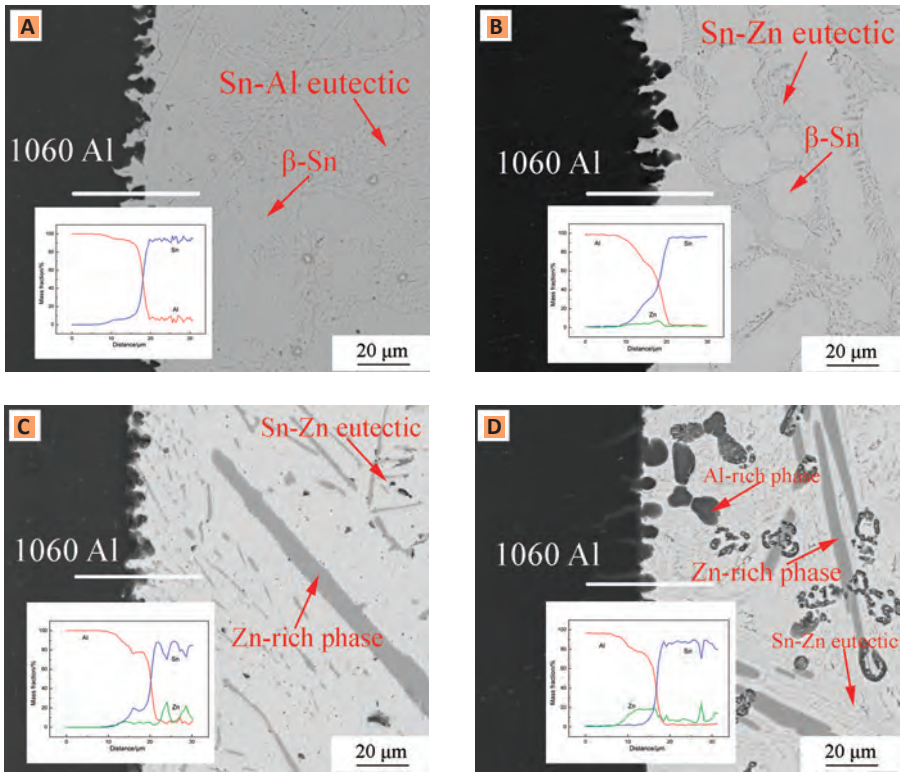

Fig. 3 — Interface morphology and corresponding EDS line-scanning result of joints soldered with A — pure Sn; B — Sn-4Zn; C — Sn-9Zn; D — Sn-20Zn.

Mechanical Properties

Tensile tests were used to evaluate the mechanical properties of joints. The black line in Fig. 4 shows the tensile strength of joints with different filler metals. The joint soldered with pure Sn has a tensile strength of 63± 2.8 MPa. When Zn was added to the filler metal, the tensile strength increased to more than 80 MPa. Joints with Sn-9Zn and Sn-20Zn have the same tensile strength of about 80 MPa, which approaches the strength of 1060 Al, while strength of the joint with Sn-4Zn can get as high as 86± 3.2 MPa, which is slightly higher than the base metal. As a matter of fact, if a sample of equal section is prepared for a tensile test, fracture will occur at the base metal, which means an interface stronger than the filler metal can be realized with only 4% Zn.

The red dashed line in Fig. 4 shows the possible tensile strength at the interface. Since the joint with pure Sn fails along the interface, the joint strength is also its interface bonding strength. The joints with Sn-Zn solders all fail in the filler metal, which means the interfaces are stronger than the filler metal and their strength values cannot be obtained in the tensile test. Al 3003 was soldered with Sn-9Zn in our previous work, and a strength of 120 MPa was obtained, which means Al/Sn-9Zn interface bonding strength is more than 120 MPa. The AlZnSn solid solution layer gets thicker when Zn is increased, so the interface may also be stronger with more Zn.

The blue line in Fig. 4 shows the relationship between elongation and content of Zn. The joint with pure Sn shows typical interface fracture, and bonding of the interface is so weak that the joint fractured before much deformation. Joints with hypereutectic Sn-Zn filler metals also show inter-

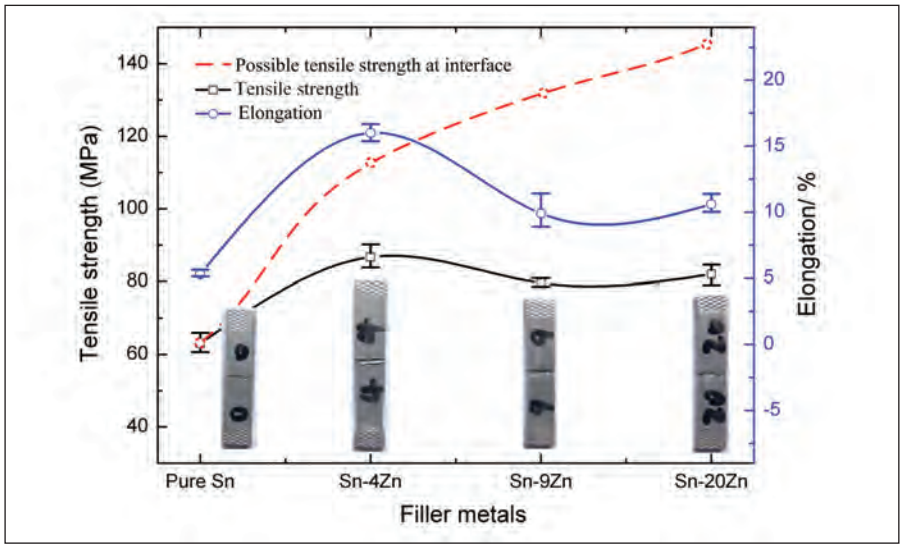

Fig. 4 — Relationship between content of Zn and mechanical properties of joints.

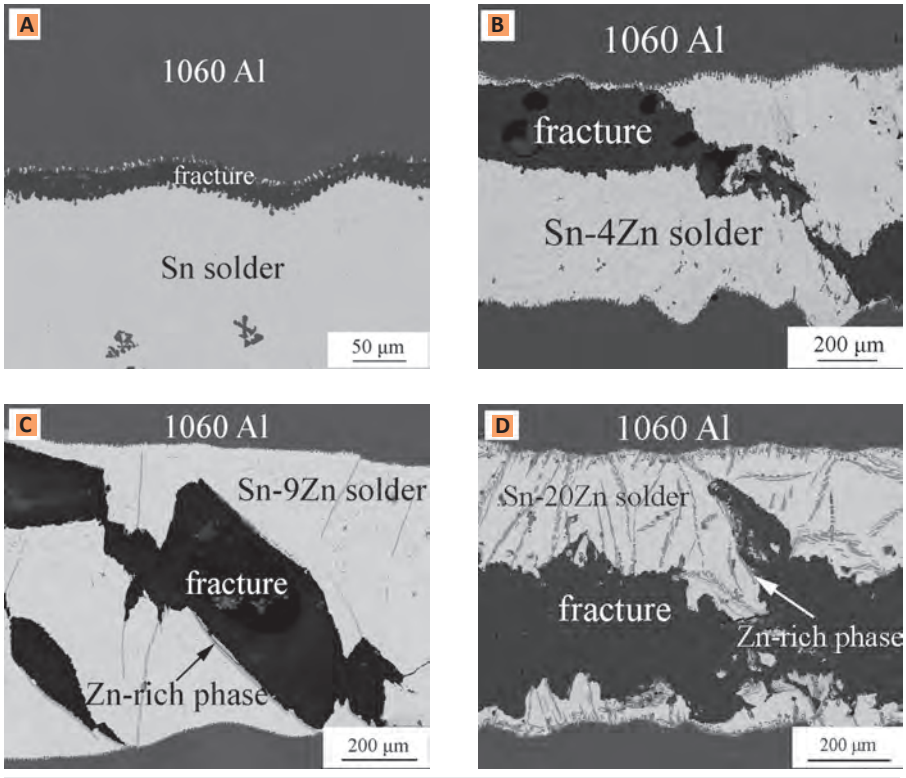

Fig. 5 — Fracture location of joints soldered with A — pure Sn; B — Sn-4Zn; C — Sn-9Zn; D — Sn-20Zn.

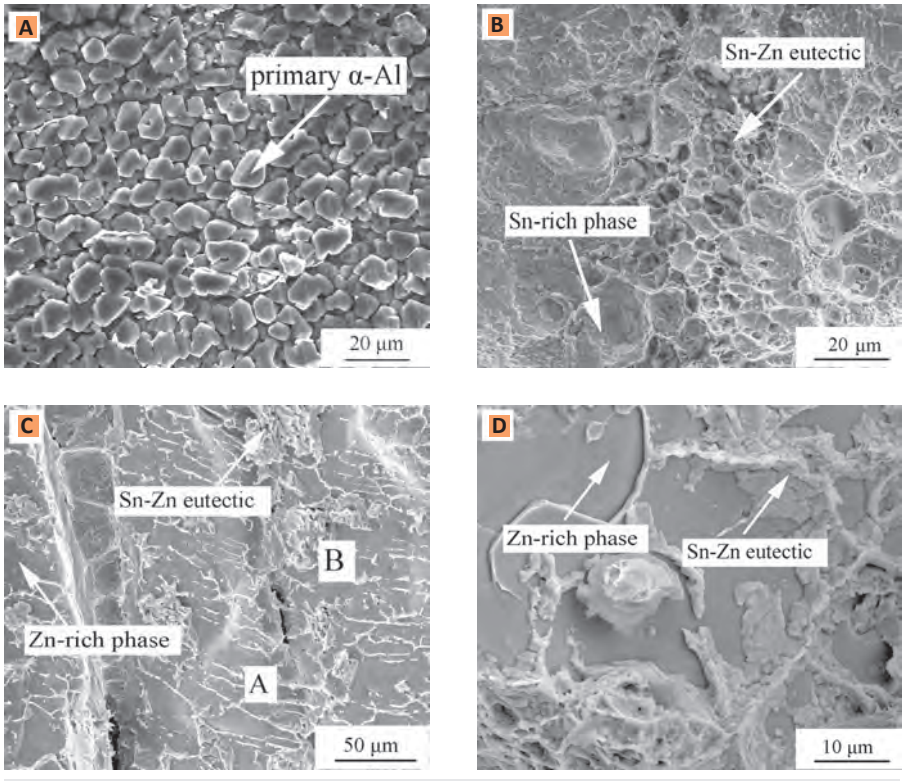

Fig. 6 — Fracture surface of joints soldered with A — pure Sn; B — Sn-4Zn; C — Sn-9Zn; D — Sn-20Zn.

face fracture, but the interface was already strengthened, and bonding between Zn-rich and Sn-Zn eutectic phases is much stronger than that of Sn/Al interface. Strength of the joints approaches the strength of the base metal, so the joints experienced large deformation before failure. As to the joint with Sn-4Zn, the interface is stronger than the filler metal and no other weak interface exists in the bond zone, so it shows typical ductile fracture and has the highest elongation.

Failure Behaviors

Figure 5 shows cross sections of the fractured region with different filler metals. The joint with pure Sn shows a typical interfacial failure type — Fig. 5A. The fracture initiates at Al/Sn interface during the tensile test and then partially turns into the filler metal layer, which indicates that the joint tensile strength has a close relationship with Al/Sn interface strength. The Al/Sn interface is the weakest area of the joint for the low degree of element diffusion. Figure 5B shows fracture path of the joint with Sn-4Zn. With only 4% Zn, tensile strength raised to more than 80 MPa, and fracture occurs in the filler metal layer rather than Al/Sn inteface. It can be concluded that the interface has been strengthened by Zn. Fracture initiates from the solder near the interface, and then turns into the other side. Figure 5C, D shows the fracture paths of joints with Sn-9Zn and Sn-20Zn. They present almost the same fracture behavior, and the joints fail along the interface of Zn-rich and Sn-Zn eutectic phases rather than Al/Sn interface. For larger solubility of Al and Zn, the diffusion layer at the interface will be thicker with more Zn. The interface would be Al/AlZnSn solid solution/Sn-Zn eutectic or b-Sn phase instead of the weak interface of Al/Sn. Thus, interface strength is improved significantly. Then the interface of Zn-rich and Sn-Zn eutectic phase becomes the weakest area of the joint.

Figure 6 shows the fracture surfaces of tensile failed joints with different filler metals. For the joint with pure Sn, the fracture surface of Al side (Fig. 6A) shows the 3-D morphology of primary a-Al particles at the interface. All of them tend to be enclosed with {111}

faces. Typically, aluminum has a fcc crystal structure, and the surface energy ranking of Al crystal faces runs as g{110}>g{100}>g{111} (Ref. 27). Primary a-Al would like to expose its {111} faces in liquid tin to minimize total surface free energy, thus presenting regular facet morphology. The fracture surface of the solder side presents regular pits corresponding to a-Al particles. Figure 6B shows the fracture surface of the Sn-4Zn joint. The fracture propagates in the filler metal layer, and fracture surface shows b-Sn and Sn-Zn eutectic phase, both of which have lots of dimples with different sizes. This indicates that it is typical ductile fracture. Figure 6C and D shows the fracture surfaces of joints with Sn-9Zn and Sn-20Zn. Since joints fail along the interface of Zn-rich and Sn-Zn eutectic phase, fracture surfaces all show Zn-rich and Sn-Zn eutectic phases. The chemical composition of point A at surface is Zn: 92.38%, Sn: 7.62%; point B Zn: 9.96%, Sn: 90.04%, which are Zn-rich and Sn-Zn eutectic phases, respectively. The Zn-rich phase is plate-like in space with a smooth surface, and there is still some Sn-Zn eutectic phase on the Zn-rich phase.

Discussion

Microstructure and fracture path models (Fig. 7) of joints soldered with pure Sn, hypoeutectic Sn-4Zn, and hypereutectic Sn-20Zn were established based on the results above. It can be concluded that Al does not react with Sn and Zn at all, and metallic bonding between Al and Sn-based solder rely on the solid solution formed at the interface. But Al and Sn form only a very thin solid solution to strengthen the interface. Therefore, the strength of Al/Sn interface is quite low, and the joint will fail along the interface, as shown in Fig. 7A. The shear strength was about 30–60 MPa and varied from base metals and process parameters based on the literature (Refs. 13, 19, 21), as discussed in the introduction.

Tensile strength of 63± 2.8MPa was obtained in this work. Whereas, Zn and Al have relatively larger mutual solubility, there was a thick layer of Al-Zn solid solution at the interface when Al alloys were soldered with Zn-Al filler metal (Ref. 28), and the tensile strength could reach 130–200 MPa (Ref. 8), which is much higher than that of Al/Sn joints. As to results in this work, it is found that Zn can strengthen Al/Sn interface by the formation of AlZnSn solid solution, and an interface stronger than filler metal can be realized with only 4% Zn. The fracture crosses Sn-rich and Sn-Zn eutectic phases — Fig. 7B. The joints have the highest strength and ductility, and as shown in Fig. 7C, a Zn-rich phase would appear if hypereutectic Sn-Zn solder was used. The interfaces of Zn-rich and Sn-Zn eutectic phases weaken the strength of the joints slightly. Almost equal tensile strength would be obtained with hypereutectic Sn-Zn solder with different Zn content for the existence of Zn-rich/Sn-Zn eutectic phase interface. Nagaokao (Ref. 12) also got tensile strength at the same level with hypereutectic Sn-xZn (x = 9, 23, 40, 82) filler metals. Beside, adding too much Zn would raise the liquidus temperature of the solder, so the hypoeutectic Sn-Zn solder is most suitable for soldering of 1060 Al, and a joint with best strength and ductility can be obtained.

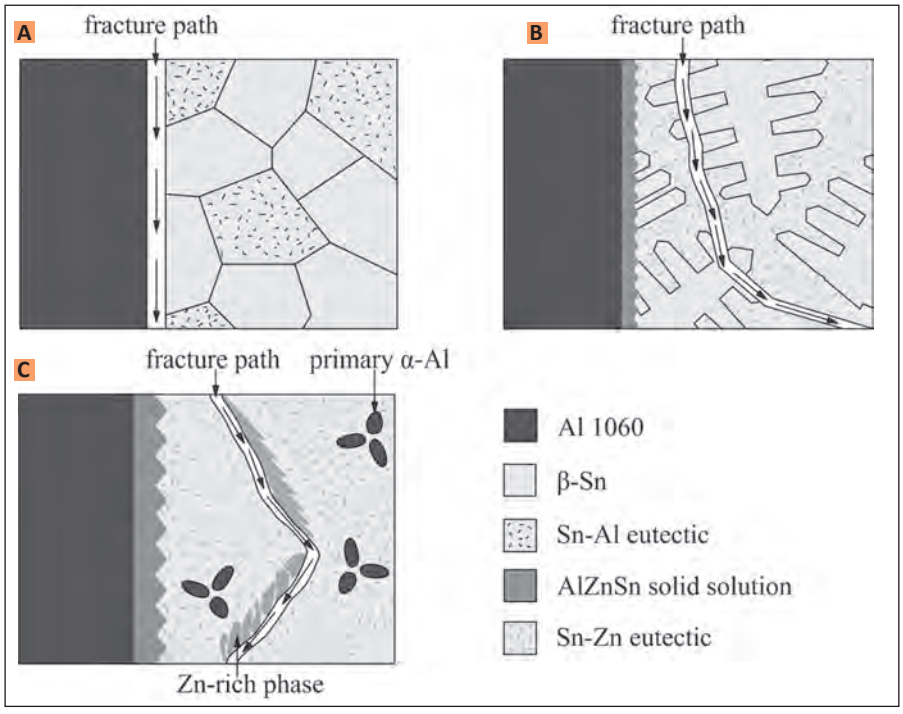

Fig. 7 — Microstructure and fracture paths model of joints soldered with A — pure Sn; B — Sn-4Zn; C — Sn-20Zn.

Conclusions

Pure Sn and Sn-Zn solders with different Zn contents were used to ultrasonic solder 1060 Al at 300°C without flux. Ultrasonic waves contribute to the breakage of oxide film, and could promote wetting and metallic bonding between the solder and 1060 Al. Joints with good interface bonding were realized with all the filler metals. Bonding between Al and Sn is weak and fracture occurs at the Al/Sn interface during tensile testing. The tensile strength is 63± 2.8 MPa. Zn would segregate at the interface for larger mutual solubility of Zn and Al, which can strengthen the interface significantly by forming a layer of AlZnSn solid solution. With an increase of Zn, the pre-eutectic phase of the metallic bond zone transforms from Sn-rich phase to Zn-rich phase. Joints all fail along the interface of the Zn-rich and Sn-Zn eutectic phases, thus the content of Zn does not affect the strength of joints with hypereutectic solder. An interface stronger than filler metal and best ductility can be realized with only 4% Zn.

Acknowledgment

This research was sponsored by the Natural Science Foundation of China (Grant No. 51105106).

References

1. Wu, S. C., Yu, X., Zuo, R. Z., Zhang, W. H., Xie, H. L., and Jiang, J. Z. 2013. Porosity, element loss, and strength model on softening behavior of hybrid laser arc welded Al-Zn-Mg-Cu alloy with synchrotron radiation analysis. *Welding Journal* 92(3): 64-s to 71-s.

2. Shi, C. J., Mao, W. M., and Chen, X. G. 2013. Evolution of activation energy during hot deformation of AA7150 aluminum alloy. *Materials Science and Engineering* A 571: 83–91.

3. Gould, J. E. 2012. Joining aluminum sheet in the automotive industry — A 30-year history. *Welding Journal* 91(1): 23-s to 34-s.

4. Xiao, Y., Ji, H. J., Li, M. Y., and Kim, J. Y. 2013. Ultrasound-assisted brazing of Cu/Al dissimilar metals using a Zn-3Al filler metal. *Materials & Design* 52: 740–747.

5. Dai, W., Xue, S. B., Lou, J. Y., and Wang, S. Q. 2012. Development of Al-Si-Zn-Sr filler metals for brazing 6061 aluminum alloy. *Materials & Design* 43: 395–402.

6. Chang, S. Y., Tsao, L. C., Li, T. Y., and Chunag, T. H. 2009. Joining 6061 aluminum alloy with Al-Si-Cu filler metals. *Journal of Alloys and Compounds* 488(1): 174–180.

7. Nagaoka, T., Morisada, Y., Fukusumi, M., and Takemoto, T. 2011. Selection of soldering temperature for ultrasonic-assisted soldering of 5056 aluminum alloy using Zn-Al system solders. *Journal of Materials Processing Technology* 211(9): 1534–1539.

8. Weiss, M., Taylor, A. S., Hodgson, P. D., and Stanford, N. 2013. Strength and biaxial formability of cryo-rolled 2024 aluminium subject to concurrent recovery and precipitation. *Acta Materialia* 61(14): 5278–5289.

9. Mahathaninwong, N., Plookphol, T., Wannasin, J., and Wisutmethangoon, S. 2012. T6 heat treatment of rheocasting 7075 Al alloy. *Materials Science and Engineering* A 532:91–99.

10. Wang, K. K., Kang, Y. L., Song, P. G., Xu, F., and Li, X. H. 2010. Preparation of SiCp/A356 electronic packaging materials and its thixo-forging. *Transactions of Nonferrous Metals Society of China* 20: 988–992.

11. Hahnlen, R., Fox, G., and Dapino, M. 2012. Ultrasonic soldering of shape memory NiTi to aluminum 2024. *Welding Journal* 91(1): 1-s to 7-s.

12. Nagaoka, T., Morisada, Y., Fukusumi, M., and Takemoto, T. 2009. Joint strength of aluminum ultrasonic soldered under liquidus temperature of Sn-Zn hypereutectic solder. *Journal of Materials Processing Technology* 209(11): 5054–5059.

13. Li, Y. X., Leng, X. S., Cheng, S., and Yan, J. C. 2012. Microstructure design and dissolution behavior between 2024 Al/Sn with the ultrasonic-associated soldering. *Materials & Design* 40: 427–432.

14. Chen, X. G., Yan, J. C., Gao, F., Wei, J. H., Xu, Z. W., and Fan, G. H. 2013. Interaction behaviors at the interface between liquid Al–Si and solid Ti-6Al-4V in ultrasonic-assisted brazing in air. *Ultrasonics Sonochemistry* 20(1): 144–154.

15. Xiao, Y., Ji, H. J., Li, M. Y., Kim, J. Y., and Kim, H. B. 2013. Microstructure and joint properties of ultrasonically brazed Al alloy joints using a Zn-Al hypereutectic filler metal. *Materials & Design* 47: 717–724.

16. Nagaoka, T., Morisada, Y., Fukusumi, M., and Takemoto, T. 2010. Ultrasonic-assisted soldering of 5056 aluminum alloy using quasi-melting Zn-Sn alloy. *Metallurgical and Materials Transactions* B 41(4): 864–871.

17. Elrefaey, A., Wojarski, L., Pfeiffer, J., and Tillmann, W. 2013. Preliminary investigation on ultrasonic-assisted brazing of titanium and titanium/stainless steel joints. *Welding Journal* 92(5): 148-s to 153-s.

18. Wei, J. H., Deng, B. H., Gao, X. Q., Yan, J. C., and Chen, X. G. 2013. Interface structure characterization of Fe36Ni alloy with ultrasonic soldering. *Journal of Alloys and Compounds* 576: 386–392.

19. Faridi, H. R., Devletian, J. H., and Le, H. 2000. A new look at flux-free ultrasonic soldering. *Welding Journal* 79(9): 41–45.

20. Diao, H., Wang, C. Q., and Wang, L. 2008. Bonding of aluminum alloy by hot-dipping tin coating. *Advanced Materials Research* 32: 93–98.

21. Ding, M., Zhang, P. L., Zhang, Z. Y., and Yao, S. 2010. Direct-soldering 6061 aluminum alloys with ultrasonic coating. *Ultrasonics Sonochemistry* 17(2): 292–297.

22. Sugo, H., Kisi, E., and Cuskelly, D. 2013. Miscibility gap alloys with inverse microstructures and high thermal conductivity for high energy density thermal storage applications. *Applied Thermal Engineering* 51(1): 1345–1350.

23. Puga, H., Costa, S., Barbosa, J., Ribeiro, S., and Prokic, M. 2011. Influence of ultrasonic melt treatment on microstructure and mechanical properties of $AlSi_9Cu_3$ alloy. *Journal of Materials Processing Technology* 211(11): 1729–1735.

24. Chen, X. G., Yan, J. C., Ren, S. C., Wei, J. H., and Wang, Q. 2013. Microstructure and mechanical properties of Ti-6Al-4V/Al1060 joints by ultrasonic-assisted brazing in air. *Materials Letters* 95: 197–200.

25. Osorio, W. R., Peixoto, L. C., Garcia, L. R., Mangelinck-Noël, N., and Garcia, A. 2013. Microstructure and mechanical properties of Sn-Bi, Sn-Ag and Sn-Zn lead-free solder alloys. *Journal of Alloys and Compounds* 572: 97–106.

26. Protasova, S. G., Kogtenkova, O. A., Straumal, B. B., Zieba, P., and Baretzky, B. 2011. Inversed solid-phase grain boundary wetting in the Al-Zn system. *Journal of Materials Science* 46(12): 4349–4353.

27. Smith, J. R., and Banerjea, A. 1987. New approach to calculation of total energies of solids with defects: Surface-energy anisotropies. *Physical ReviewLetters* 59(21): 2451–2454.

28. Li, Y. X., Zhao, W. W., Leng, X. S., Fu, Q. J., Wang, L., and Yan, J. C. 2011. Microstructure evolution and mechanical properties of ultrasonic-assisted soldering joints of 2024 aluminum alloys. *Transactions of Nonferrous Metals Society of China* 21(9): 1937–1943.